Development of the axonal βII-spectrin periodic skeleton requires active cytoskeletal remodelling

Shivani Bodas[1], Ashish Mishra[2], Pramod Pullarkat[2] and Aurnab Ghose[1,*]

[1] Indian Institute of Science Education and Research (IISER) Pune, Dr. Homi Bhabha Road, Pune 411008, India.

[2] Raman Research Institute, C. V. Raman Avenue, Bengaluru 560 080, India

[*] Correspondence: aurnab@iiserpune.ac.in

Running head: Development of the axonal βII-spectrin MPS

Keywords: βII-spectrin; membrane-associated periodic skeleton (MPS); F-actin; microtubule; STED

ABSTRACT

The axonal membrane-associated periodic skeleton (MPS), consisting of F-actin rings crosslinked by spectrin heterotetramers, is ubiquitous and critical for neuronal function and homoeostasis. However, the initiation and early development of the axonal MPS are poorly understood. Using superresolution imaging, we show that βII-spectrin is recruited early to the axonal cortex, followed by progressive establishment of long-range periodic order. Microtubule dynamics are essential for MPS formation in the early stages, but transition to a passive stabilising role in mature axons. We show that the early subplasmalemmal recruitment of βII-spectrin is dependent on cortical actin but not on actomyosin contractility, and active nucleation of F-actin is required in early development but is dispensable for the mature MPS. Using a βII-spectrin knockout model, we demonstrate that the actin-binding and lipid-interacting domains of βII-spectrin are critical for its subplasmalemmal confinement and, subsequently, MPS maturation. These findings highlight stage-specific cytoskeletal remodelling underlying MPS development and advance our understanding of axonal subcellular architecture.

INTRODUCTION

The axonal subplasmalemmal membrane periodic skeleton (MPS) is ubiquitous across phyla and forms a quasi-1d lattice along the entire neuronal axon (D'Este et al., 2016; He et al., 2016). A similar scaffold is found in dendrites and dendritic spine necks (Han et al., 2017). The MPS comprises of axially aligned tetramers of α and β spectrins that are attached to evenly distributed radial F-actin rings, which maintain a typical spacing of 180 – 190 nm (Xu et al., 2013). The lattice acts as a load-bearing scaffold, providing mechanical support to the plasma membrane (Hammarlund et al., 2007; Dubey et al., 2020). The MPS plays an essential role in the maintenance of axonal homoeostasis, regulating the ion channel distribution, maintaining the axonal diameter and facilitating axonal transport (Costa *et al.*, 2020a; Wang *et al.*, 2020a).

Furthermore, the MPS acts as a signalling scaffold (Zhou et al., 2019) , limits diffusion at the axon initial segment (Albrecht et al., 2016), modulates endocytosis (Wernert et al., 2024) and is linked to axon degeneration (Unsain et al., 2018; Wang et al., 2019). Studies in *C. elegans*, mice and humans have revealed that impairment of the MPS leads to a variety of defects and lethality(Hammarlund et al., 2007; Huang et al., 2017a; b; Lorenzo et al., 2019; Cousin et al., 2021).

Despite the explosion of interest in the axonal MPS, its early development and maintenance are not well understood. Cytoskeleton dependence on MPS stability has been typically studied in late-stage neurons and does not address early functions in initiating MPS development. The depolymerisation of F-actin inhibits MPS development in early axons (Xu et al., 2013; Zhong et al., 2014) and destabilises mature MPS (Qu et al., 2017; Unsain et al., 2018). However, what functions are subserved by F-actin in MPS initiation are unclear. Similarly, while microtubule integrity appears to be necessary for MPS maintenance (Zhong et al., 2014; Qu et al., 2017), its function in MPS development is unknown.

We present a chronological analysis of the βII-spectrin MPS development in embryonic DRG neurons using STED nanoscopy. Our findings reveal that βII-spectrin is recruited early to the axonal cortex and progressively matures to attain long-range periodic order and uniform spacing. In the early stages, microtubule dynamics are essential for MPS formation, but microtubules have a passive function in stabilising the mature MPS. We show that βII-spectrin is recruited to the axonal cortex via interactions with subplasmalemmal F-actin, and the early MPS is dependent on actively nucleating actin networks. However, the mature, stable MPS is insensitive to the inhibition of F-actin nucleation. Using βII-spectrin knockout cells, we demonstrate that the actin-binding and PH-domains of βII-spectrin are necessary for its recruitment to the axonal cortex.

MATERIALS AND METHODS

Primary neuronal cultures

All experimental procedures were conducted in accordance with guidelines approved by the Institutional Animal Ethics Committee of the Indian Institute of Science Education and Research (IISER) Pune, India. Fertilised White Leghorn chicken eggs were obtained from Venkateshwara Hatchery Private Limited (Pune, India) and were incubated at 37 °C in a humidified incubator for 8-9 days.

Dorsal root ganglia (DRG) were isolated from embryos using sterile Leibovitz's L-15 medium (Hi-Media, AL204A) for dissection. Dissections were performed in a laminar flow hood. Around 12-16 DRGs were isolated per embryo in the L-15 medium. The suspension was centrifuged at 3000 rpm for 3 min and the supernatant was removed. The DRGs in the pellet were resuspended in trypsin solution and incubated for 30 min at 37 °C. This was followed by a 3-minute spin at 3000 rpm to remove most of the trypsin solution and an L-15 wash to remove any remaining trypsin. The dissociated neurons were then plated onto glass coverslips or Poly-D-lysine-coated (0.1 mg/ml PDL; Merck, A-003-E) glass-bottom dishes. Neurons were cultured in serum-free medium composed of L-15 supplemented with 6 mg/ml glucose, 1× GlutaMAX (Gibco, 35050061), 1× B27 supplement (Invitrogen, A1895601), 50 ng/ml nerve growth factor (Gibco, 13290010), 0.006 g/ml methyl cellulose (34516, ColorconID), and 1× PenStrep (HiMedia, A001A). Cultures were maintained in a non-CO2 incubator at 37 °C.

Drug treatment of neurons

The specific drugs utilised, along with their corresponding treatment conditions, are described in the table below. All the cultures were fixed and processed for immunofluorescence analysis at different time points. All drugs were prepared in dimethyl sulfoxide (DMSO), and DMSO-treated cultures served as vehicle controls for each drug treatment.

Drug	Source	Type of treatment	Time of addition	Concentration	Duration
Taxol	Santa Cruz (sc-201439)	Acute	DIV 1,2 & 4	10 μM	30 min
Nocodazole	Tocris Bioscience (2792)	Acute	DIV 1,2 & 4	20 μM	30 min
Latrunculin-A	Sigma Aldrich (L5163)	Acute	DIV 1,2 & 4	5 μM	15 min
Jasplakinolide	Tocris Bioscience (1228)	Acute	DIV 1,2 & 4	5 μM	30 min
Taxol	Santa Cruz (sc-201439)	Chronic	16 hrs post seeding	1 nM	Till DIV 2 or 4
Nocodazole	Tocris Bioscience (2792)	Chronic	16 hrs post seeding	10 nM	Till DIV 2 or 4
Jasplakinolide	Tocris Bioscience (1228)	Chronic	16 hrs post seeding	10 nM	Till DIV 2 or 4
Blebbistatin	Sigma Aldrich (B0560)	Chronic	16 hrs post seeding	10 μM	Till DIV 2 or 4
CK666	Merck (182515)	Acute	DIV 2,4 & 6	20 μM	30 min

SMIFH2	Merck (344092)	Acute	DIV 2,4 & 6	20 µM	30 min

111

112 **Cell fixation and immunostaining for fluorescence imaging**

113 Cultured neurons were fixed in 4% (w/v) paraformaldehyde (PFA) in phosphate-
114 buffered saline (PBS) for 10 min at room temperature (RT). PFA was removed by
115 washing with PBS, and the cells were then permeabilised with 0.1% (v/v) Triton X-
116 100 in PBS for 5 min at RT, followed by blocking in 3% (w/v) bovine serum albumin
117 (BSA) in PBS for 1 hr at RT. The cells were then incubated with the primary
118 antibodies – (βII-spectrin 1:700 (BD Biosciences; 612563), Anti-GFP 1:500
119 (Invitrogen; A11122) and βIII-tubulin 1:1000 (Santa-Cruz; sc-80005)) - overnight at 4
120 °C. The primary antibodies were removed the following day, followed by 3x PBS
121 washes, and the cells were incubated with the secondary antibodies – Alexa 488
122 conjugated anti-mouse or anti-rabbit (Invitrogen; A-11001, A-11008, respectively) –
123 at 1:1000 dilution in blocking buffer for 1 hr at RT. For super-resolution microscopy,
124 neurons at different stages of *in vitro* culture (days in vitro or DIV) were mounted in a
125 mixture of 10% Mowiol 4–88 in poly (vinyl alcohol) (Sigma-Aldrich, 81381) and 2.5%
126 (w/v) DABCO (1,4-diazabicyclo [2.2.2] octane; Sigma-Aldrich, D27802). The
127 mounted samples were stored overnight in the dark at 4 °C before imaging.

128 **Plasmid construction and transfection**

129 Human βII-Spectrin (from Addgene plasmid 31070: βII-Spectrin-HA) was incorporated
130 into a pCAG-GFP containing vector by PCR. For the actin-binding deletion mutant
131 (pCAG-ΔABD-βII-Spectrin-GFP) initial 3-277 aa was deleted from the pCAG-βII-
132 Spectrin-GFP construct by PCR. Plasma membrane binding mutant (pCAG-βII-
133 Spectrin-K2207Q-GFP) and Ankyrin binding mutant (pCAG-βII-Spectrin-Y187A-GFP)
134 were created by introducing point mutations in the pCAG-βII-Spectrin-GFP construct
135 by PCR. Cells were suspended in Optimem® (Gibco) medium with 15-20 µg of
136 plasmid. Subsequently, the cell suspension was electroporated using the Nepagene
137 NEPA21 Type II machine. The following parameters were used in all experiments:
138 Poring pulse: 2x of 5 msec 125 V pulses with pulse interval of 50 msec and decay rate
139 of 10%; polarity +. Transfer pulse: 5x of 50 msec 20 V pulses with pulse interval of 50
140 msec and decay rate of 40%; polarity +/-. After electroporation, the cells were seeded
141 in glass-bottom dishes and incubated at 37 °C for relevant periods.

142 **βII-Spectrin intensity analysis**

143 Axons from DIV 1, 2, and 4 were stained for βII-Spectrin and imaged using confocal
144 microscopy. The middle region of the axon was selected and processed with ImageJ
145 software for Otsu-based thresholding. A particle analyser tool was used to estimate
146 the integrated density and area of the axon, followed by CTCF calculation.

147 **Fluorescence recovery after photobleaching & analysis**

148 Primary neurons and differentiated βII-Spectrin KO SH-SY5Y cells were transfected
149 via electroporation and used in experiments at various time points, ranging from 24
150 to 144 hr post-transfection. The following plasmids were used for transfection:
151 pCAG-βII-Spectrin-GFP, pCAG-βII-Spectrin-K2207Q-GFP, pCAG-βII-Spectrin-
152 Y187A-GFP, and pCAG-ΔABD-βII-spectrin-GFP.

153 Fluorescence recovery after photobleaching (FRAP) experiments were conducted
154 using a Zeiss LSM 710 confocal microscope equipped with a 488 nm Argon laser for

bleaching and a 37 °C humidified stage. Time-lapse images of GFP fluorescence were acquired at 2-second intervals using a Zeiss Plan-Apochromatic 63x/1.4 Oil objective with 3× optical zoom. Regions of interest (ROI) measuring a maximum of ~2 × 1 microns (height × width) along the middle of the axon were iteratively photo-bleached (50-100 iterations) by scanning with a 488 nm laser at 100% power and a scanning speed of 6 µs/pixel. Post-bleach images were acquired with 15–30% laser intensity for 150 frames (2 second interval). The resulting images were analysed using the ImageJ software.

For each region of interest (ROI), background fluorescence was subtracted at each time point. A reference region was used to correct for fluorescence loss due to bleaching during image acquisition by normalising it to the pre-bleaching intensity. The background-corrected and acquisition-loss-corrected ROI intensities were then further normalised by setting the pre-bleaching intensity to 100% and the immediate post-bleaching intensity to 0%. The recovery curve was fitted to a single-phase association function from data plotted with a 2s or 10s interval. The extra sum-of-squares F-test was used to compare the plateaus of the curves. The half-life ($t_{½}$) was estimated from the fitted curve of individual axons, and the % mobile fraction was calculated by averaging the last 5 frames of the recovering curve.

SH-SY5Y Neuroblastoma cell differentiation and culture

SH-SY5Y cells were grown and maintained in 60 mm Petri dishes in standard culture medium (DMEM/F12 supplemented with 10% fetal bovine serum [FBS] and 1% penicillin-streptomycin) at 37 °C in a 5% CO2 atmosphere. Cells were passaged upon reaching 80–90% confluence using trypsin-EDTA, and all experiments were conducted using cells with a passage number below 20. SH-SY5Y cells were differentiated into neuron-like cells over 12-14 days of Retinoic acid (RA) and Brain-derived neurotrophic factor (BDNF) treatment. Briefly, cells were seeded in a surface-coated 60 mm flask and treated with retinoic acid in DMEM/F12 supplemented with 1% FBS for 5 days, followed by 8 days of brain-derived neurotrophic factor (BDNF) treatment in serum-free medium.

For FRAP and STED microscopy, cells were trypsinised, transfected with the appropriate plasmids, and then reseeded on glass-bottomed, surface-treated dishes after RA treatment. They were maintained in serum-free BDNF-supplemented media for 6 days, and experiments were performed.

CRISPR/CAS9-mediated gene editing

Using an online CRISPR design tool (Ran et al., 2013), two pairs of oligo DNAs encoding gRNAs were designed to target βII-Spectrin exon 16 sequences (gRNA 1: 5′-CCAGACAGCGATCGCCTCGGAGG-3′ and gRNA 2: 5′-GAACGAGATCGACAACTACGAGG-3′**.** These oligos were synthesised, annealed, and inserted into the BbsI site of the pSpCas9(BB)-2A-GFP (PX458) plasmid (Addgene plasmid no.48138). The resulting plasmids were amplified and introduced into SH-SY5Y cells via electroporation. GFP-positive cells were isolated through cell sorting. Western blot analysis was used to initially identify stably transfected clonal lines exhibiting complete depletion of SH-SY5Y expression.

Indel analysis of βII-Spectrin knockout cell lines

To examine indel mutations in SH-SY5Y βII-Spectrin knockout cells, genomic DNA was extracted from the knockout clonal lines. Subsequently, PCR amplification of exon 16 was performed using the extracted genomic DNA as a template. The

202 following oligonucleotides were used as primers: forward 5′-
203 CCCTGAAAAACCGAGAGGCC-3′ and reverse 5′-GCTCGTTCCATCCAGTGTCC-3′.
204 The amplified DNA was then purified, and the resulting plasmids were sequenced to
205 identify indel mutations.

206 **STED imaging & analysis**

207 STED imaging was conducted using a Leica TCS SP8 STED 3x microscope (Leica
208 Microsystems) on medial axonal segments of embryonic chick DRG neurons and
209 differentiated SH-SY5Y neurons. Images were captured with an HC PL APO CS2
210 100x/1.4 STED WHITE oil immersion objective (Leica Microsystems) in both
211 confocal and STED modes. Acquisition settings included 16x line averaging and
212 detector gating on a Hybrid Detector (HyD, Leica Microsystems) with a range of 0.3
213 ns to 8 ns. The zoom factor was set to ~6x, with a pixel size of up to 20 nm. A 592
214 depletion laser was used for all image acquisitions. All other settings were kept
215 constant.

216 Images were deconvolved using Huygens Professional software prior to analysis.
217 Medial axonal regions were segmented into ~3 µm sections, and intensity versus
218 distance profiles were generated for each segment. Autocorrelation functions using
219 MATLAB (R2021a) were computed based on the intensity profiles of each segment.
220 To obtain the average autocorrelation function, autocorrelation curves from all the
221 selected axon segments were averaged for each experimental condition. The
222 autocorrelation amplitude was defined as the difference between the first peak and
223 the average of two adjacent valleys in the averaged autocorrelation curve. The
224 average periodicity (or spacing) of the membrane periodic skeleton (MPS) structure
225 for each ~3 µm segment was determined by the position of the first peak in the
226 autocorrelation function. The diameter of each segment was calculated by
227 measuring the edge-to-edge distance between spectrin signals.

228 **Axonal ablation and analysis**

229 DRG neurons were grown on a glass-bottom dish without any coating to obtain
230 detached axons. Axons of DIV1, DIV2, and DIV4 neurons were subjected to laser
231 ablation using a home-built laser ablation setup. This setup consists of a 355 nm, 25
232 mJ, 350 ps pulsed laser (PowerChip PNV-M02510-100; Teem Photonics, Meylan,
233 France) coupled to the side port of a Leica TCS SP8 confocal microscope using a
234 custom filter-cube and focussed on the sample using a 40x/0.75 dry Phase Contrast
235 objective. A custom-made 90° rotated filter cube having a UV-reflecting dichroic filter
236 (T387lp-UF3, Chroma) was used to reflect the laser light into the objective. During
237 and after ablation, phase contrast images were recorded using a CCD camera
238 (Phantom VRI-MICRO-C210-16GB-M, Vision Research) at 2000 fps for 0.8 seconds
239 to capture the initial fast retraction process of the ablated axons. A custom MATLAB
240 code was employed to quantify the evolving gap distance. The x- and y-coordinates
241 obtained were converted to distance values and plotted using GraphPad software.
242 Estimation statistics (www.estimationstats.com), Cohen's d and a two-sided
243 permutation test between the final gap length post-ablation were determined. The F-
244 test was used to compare the plateaus of the evolving curve after fitting the data to a
245 single-phase association model.

246 **Statistical analysis**

247 All statistical analyses and visual representations were conducted using GraphPad
248 Prism 10 (10.4.0) except for Fig. S1C. In the figures, data are presented with a

central line indicating the mean, along with error bars displaying the standard error of the mean (SEM). The number of data points analysed for each graph is indicated in the figure legends. Statistical tests, along with correction tests used for the analysis, are mentioned in the figure legend. Estimation statistics (www.estimationstats.com) were used to plot the data and to calculate Cohen's d in Fig. S1C.

RESULTS

Axonal βII-spectrin progressively develops a highly periodic organisation

To investigate the developmental trajectory of the-spectrin MPS in embryonic DRG neurons, dissociated DRG neuron primary cultures were fixed at various time points, immunolabelled with βII-spectrin antibodies, and imaged using STED nanoscopy. We quantified the early development of the MPS by imaging the medial segments of axons cultured for 1, 2, 4, and 6 days *in vitro* (DIV), using autocorrelation analysis of the βII-spectrin signal (Fig. 1A,B). We quantified the degree of periodicity (autocorrelation amplitude at the first peak) and the periodic spacing of the βII-spectrin rings (periodicity) from the autocorrelation curves (Fig. 1C,D). The representative micrographs (Fig. 1A) depict the emergence and evolution of the periodic organisation of βII-spectrin in the axons across development. βII-spectrin was already localised to the axonal shaft by DIV1, but its organisation was weakly periodic (Fig. 1A). However, the average autocorrelation amplitudes increased progressively with DIV (Fig. 1B,C), indicating the consolidation of long-range periodic order. Concomitant with the increase in the extent of periodicity, the spacing (periodicity) of the βII-spectrin signal (Fig. 1D) reduced with the age of the cultured neurons from 214 ± 6.17 nm in DIV1 to 196.7 ± 2.52 nm in DIV2. It further decreased to 192.9 ± 8.9 nm and 185.8 ± 4.3 nm on DIV 4 and DIV6, respectively. The developmental maturation of the MPS was further revealed by the progressive reduction of the coefficient of variation of the βII-spectrin spacing (Fig. 1D), decreasing from 25.9 at DIV1 to 4.3 at DIV6. The high variability of the periodicities during the early stages was expectedly associated with lower autocorrelation amplitudes (Fig. 1E). The autocorrelation amplitude increased with development as the spacing converged to 185.8 ± 4.3 nm by DIV 6. Interestingly, in these axonal segments, the amount of βII-spectrin is unchanged across DIV1, 2 and 4 (Fig. S1A), though the distribution becomes highly periodic. This suggests MPS maturation is dominated by the reorganisation of spectrin, recruited to the cortex early in development, from a relatively disordered to an ordered periodic scaffold.

To evaluate whether MPS maturation across these early developmental stages influenced the axonal morphology, we measured the diameter of the βII-spectrin rings as a surrogate measure of axonal diameter. MPS maturation across DIVs correlated with a reduction in diameter (Fig.1F). This observation is consistent with the role of the MPS in regulating the axonal diameter (Costa et al., 2020; Wang et al., 2020) and suggests progressive constriction of the axonal shaft as the MPS matures. Interestingly, the decrease in diameter was already substantial by DIV2. This observation, together with a significant increase in autocorrelation amplitude (Fig. 1B) in DIV2 (compared to DIV1), suggests an early maturation of the βII-spectrin MPS in DRG neurons.

The axon is actively contractile (Mutalik et al., 2018), and the MPS has been associated with axonal tension and pre-stress (Krieg et al., 2014; Dubey et al., 2020). To assess if early MPS maturation contributes to axonal tension, we employed laser-induced axonal ablation of DIV1, 2 and 4 neurons (Fig. S1B) and followed the evolution of the gap distance between the two ends following ablation. The rate of change of the gap distance may depend on passive stresses, active contractility or progressive cytoskeletal remodelling. However, the early, exponential response is likely to be dominated by axonal pre-tension. F-test comparing the plateaus of the one-phase association fits revealed that DIV4 axons exhibit greater

pre-stress than DIV1 and DIV2 axons (Fig. 1G), while the quantitative analysis of gap distance at 0.74 seconds revealed a substantial effect size (Cohen's d=0.93; p=0.0078) compared to DIV1 (Figs. 1G, S1C). Maturation of the βII-spectrin MPS thus appears to correlate with the evolution of axonal tension. However, the change observed is modest, and there is substantial pre-tension at DIV1 when the βII-spectrin MPS is only weakly periodic.

Collectively, these data reveal the maturation kinetics of the βII-spectrin MPS in DRG axons in early development. βII-spectrin is recruited early to the axonal cortex, followed by progressive establishment of periodic order, which is concomitant with a decrease in axonal diameter and an increase in axonal pre-stress.

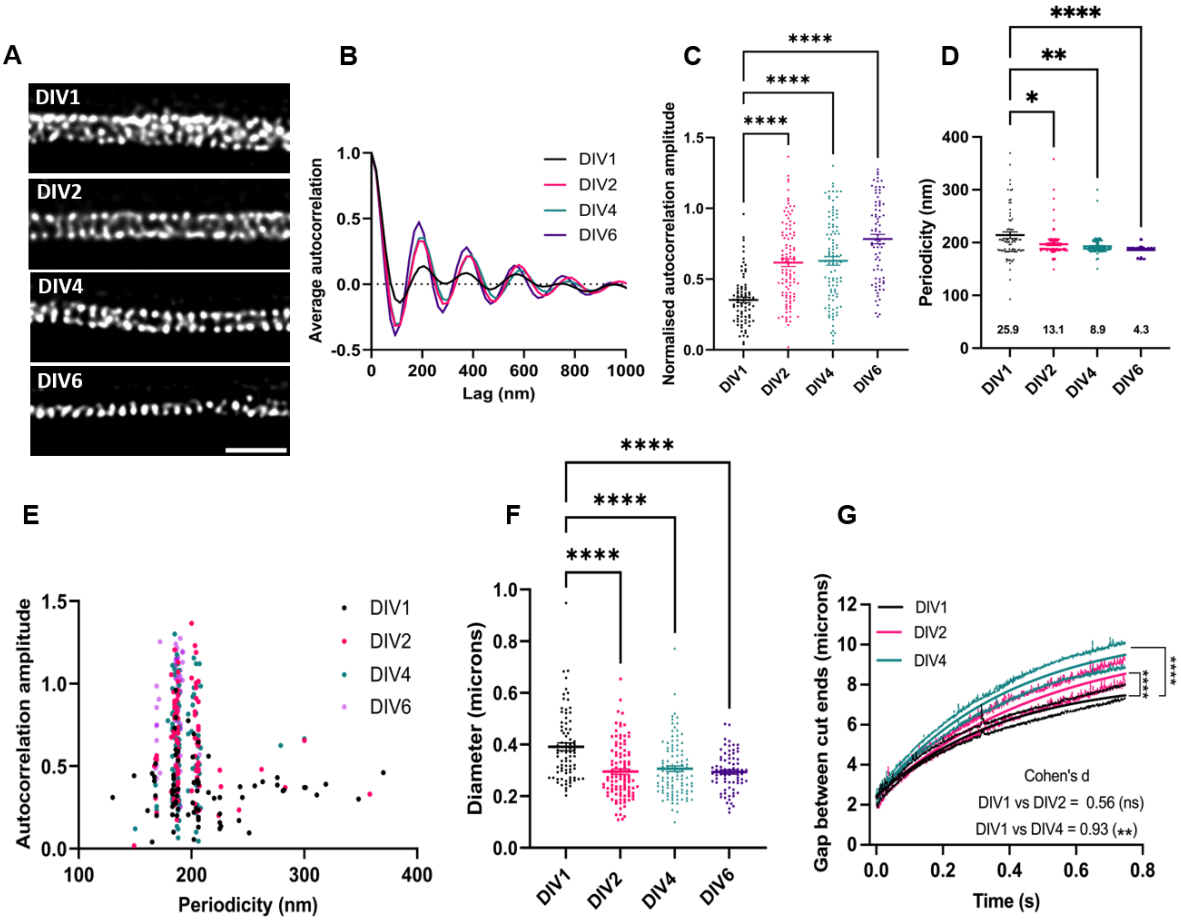

Figure 1: The βII-spectrin membrane periodic skeleton (MPS) assembles progressively. (A) Representative micrographs of single optical sections from STED nanoscopy of DIV1, DIV2, DIV4, and DIV6 DRG axons stained with βII-spectrin antibody. Scale bar: 1 µm. (B) Average autocorrelation curves across multiple axonal regions. (C) The normalised autocorrelation amplitudes of the βII-spectrin rings. Amplitudes were quantified as the difference between the first peak and the average of the first two valleys of the autocorrelation curve. The data were analysed using the Brown-Forsythe and Welch ANOVA test with multiple comparisons corrected by Games-Howell's test. (D) Periodicity across DIVs demonstrates a reduction in the spacing between the βII-spectrin rings. The data were analysed using the Brown-Forsythe and Welch ANOVA test with multiple comparisons corrected by Games-Howell's test. The numbers below each data set indicate the coefficient of variation of the distribution. (E) Plot of the normalised autocorrelation amplitudes against periodicity for all DIVs, indicating the degree of autocorrelation and the relative distribution of MPS periodicity. (F) βII-spectrin ring diameter across DIVs. The data were analysed using the Kruskal-Wallis test with multiple comparisons corrected by Dunn's test. For A-F, 80-100 axonal segments from 3 biological replicates for each DIV were analysed. (G) The evolving gap length between cut ends following ablation is represented as a one-phase fit of the means (± SEM). Curve fits were compared using the extra sum-

of-squares F-test. The effect sizes and significance, represented by Cohen's d and two-sided t-test, obtained by comparing the gap length in the last 10 frames (till 0.74 sec) using Estimation statistics (Fig S1C) are indicated. The data are derived from n=19 (DIV1), n=15 (DIV2) and n=16 (DIV4) axons from at least three biological replicates. (ns, $p > 0.05$; *, $p \leq 0.05$; **, $p \leq 0.01$; ****, $p \leq 0.0001$).

F-actin and microtubules are required for βII-spectrin MPS development

Several studies have implicated both the actin and microtubule cytoskeletal systems in the maintenance of the F-actin/βII-spectrin MPS, with most focussing on late-stage neurons. We evaluated the role of axonal F-actin and microtubules in the early development of the βII-spectrin MPS. DRG neurons at DIV1, 2, and 4 were acutely exposed to drugs that destabilised or stabilised the two cytoskeletal systems before fixation and evaluation of the βII-spectrin MPS via STED nanoscopy.

Suppression of F-actin polymerisation by latrunculin-A (Lat-A; 5 μM, 15 min) or microtubule polymerisation by nocodazole (Noco; 20 μM, 30 min) disrupted the long-range order of the periodic βII-spectrin and reduced the autocorrelation amplitudes across all DIVs (Fig. 2A-B,D-E,G-H). Furthermore, periodicity analysis revealed an increased coefficient of variation of the MPS spacing upon depolymerisation of the actin or microtubule cytoskeletons (Fig. 2C, F,I). In line with the involvement of the MPS in maintaining axon diameter, depolymerisation of F-actin or microtubules led to an increase in the diameter of the βII-spectrin rings at all DIVs (Fig. S2A, B, C).

Acute treatment with the F-actin stabilising jasplakinolide (Jasp; 5 μM, 30 min) or microtubule stabilising paclitaxel (Taxol; 10 μM, 30 min), however, did not affect the autocorrelation or average autocorrelation amplitudes at any of the DIVs (Fig. 2A-B,D-E,G-H). While the periodicity analysis revealed no difference in the mean βII-spectrin spacing, there was a notable decrease in the coefficient of variation of the spacing upon either actin or microtubule stabilisation at DIV1 but it was not obvious at DIV2 and DIV4 when the MPS is already well organised (Fig. 2C,F,I). The latter result may suggest that pharmacological stabilisation of labile F-actin and microtubules in early developmental stages facilitates the maturation of the βII-spectrin MPS. The lability of F-actin at early stages of MPS development has been previously suggested as periodic F-actin is not detectable in young hippocampal axons, though the spectrin MPS is easily discernible (Zhong et al., 2014). Stabilisation of F-actin or microtubules did not change the βII-spectrin diameter at any DIV (Fig. S2A, B, C).

These experiments demonstrate the requirement of both F-actin and microtubules in the development of the βII-spectrin MPS.

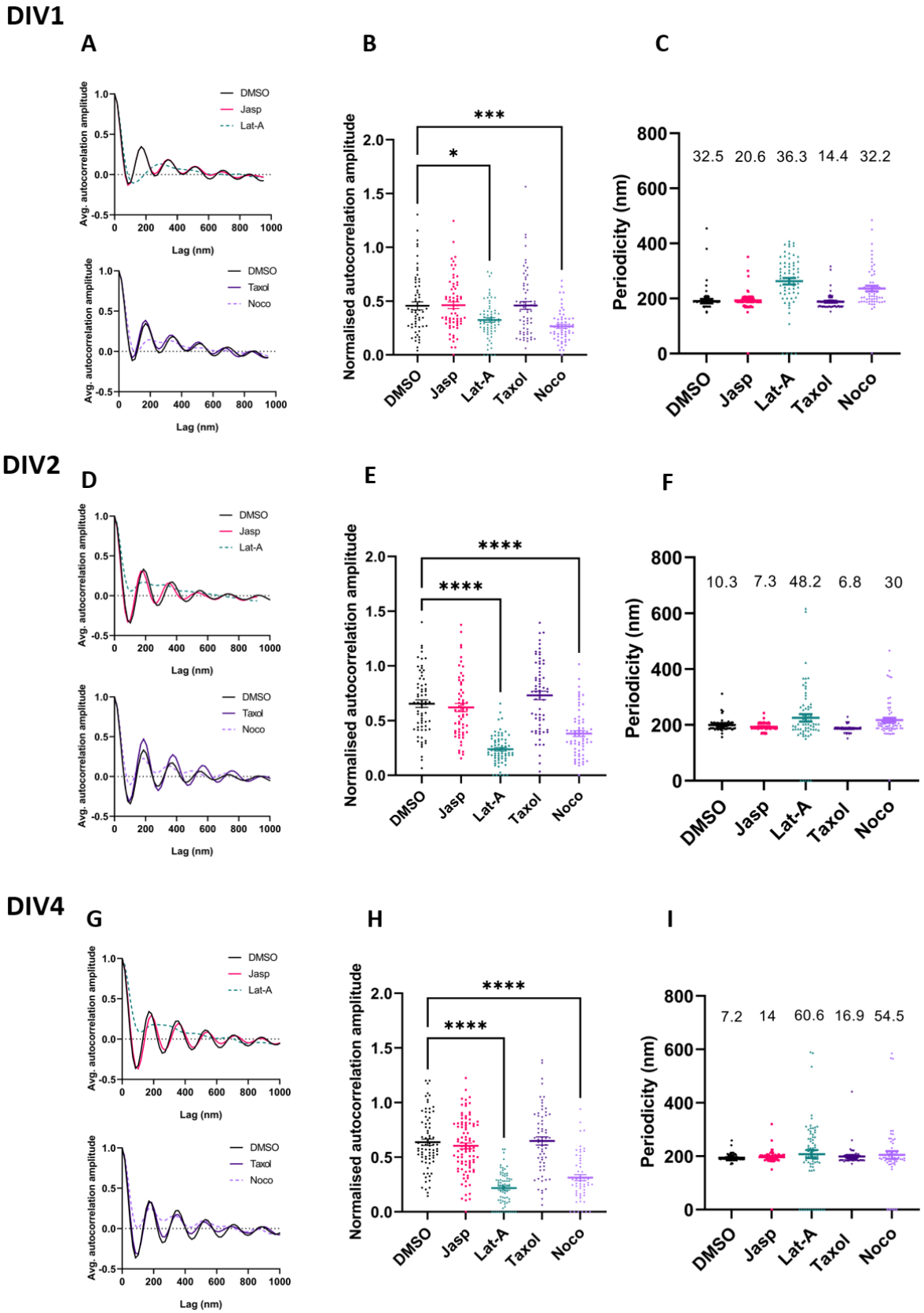

Figure 2: Destabilisation of F-actin and microtubules affects MPS development and stability. (A,D,G) Average autocorrelation curves of axonal segments across DIVs treated with DMSO (control), Jasplakinolide (Jasp), Latrunculin-A (Lat-A), Paclitaxel (Taxol), and Nocodazole (Noco). (B,E,H) The normalised autocorrelation amplitudes of the βII-spectrin rings across treatments and DIVs. The data

were analysed using the Brown-Forsythe and Welch ANOVA test with multiple comparisons corrected by Games-Howell's test (ns, $p > 0.05$; *, $p \leq 0.05$; ***, $p \leq 0.001$; ****, $p \leq 0.0001$). (C, F, I) Periodicity (spacing) across DIVs treated with indicated drugs. The numbers below each data set indicate the coefficient of variation of the distribution. The numbers above each data set indicate the coefficient of variation of the distribution. For A-I, 60-95 axonal segments from 3 biological replicates for each DIV were analysed.

Microtubule dynamics are necessary to initiate MPS development

The involvement of microtubules in destabilising the early βII-spectrin MPS (Fig. 2) led us to investigate whether microtubule dynamics were required for the initiation and consolidation of MPS. We developed an early, chronic treatment protocol where a low dose of Noco (10 nM) or Taxol (1 nM) was added 16 h post-seeding (to allow for neuritogenesis) and the cultures fixed at DIV2 and DIV4 (Fig. 3A). Chronic disruption of microtubule polymerisation by Noco disrupted MPS formation at both DIV 2 and 4, as shown by the averaged autocorrelation curves and reduced autocorrelation amplitudes (Fig. 3B-D). Interestingly, and in contrast with acute exposure to Taxol (Fig. 2), chronic stabilisation of microtubules by Taxol compromised MPS formation (Fig. 3B-D) at both DIV2 and 4. Both microtubule depolymerisation and stabilisation increased the coefficient of variation of the periodicity (Fig. 3E). The compromised MPS formation was also reflected in diameter analysis, where both Nocodazole and Taxol treatments resulted in increased axonal diameter at both DIV2 and DIV4 (Fig. S3A). Notably, despite the compromised MPS formation, the amount of βII-spectrin in these medial axonal segments remained unchanged across DIV2 and DIV4 following chronic treatment with microtubule depolymerising or stabilising agents (Fig. S3B). This observation suggests that microtubules play a critical role in facilitating the organisational plasticity of βII-spectrin, rather than the recruitment of βII-spectrin to the axons.

Chronic treatment of hippocampal neurons with paclitaxel has previously been shown to induce multiple axon-like processes with MPS (Zhong et al., 2014). However, this study was performed at later stages, and the MPS of these axon-like processes were not quantitatively evaluated. Our data suggest that a balance of stable and dynamic microtubules is required to initiate MPS formation (Fig. 3), however, the maintenance of the relatively more established MPS is only sensitive to microtubule depolymerisation (Fig.2) but not stabilisation. At later stages, microtubules appear to have a more structural function in supporting the mature MPS, but microtubule dynamics in early stages seem to be involved in the generation of periodically organised βII-spectrin.

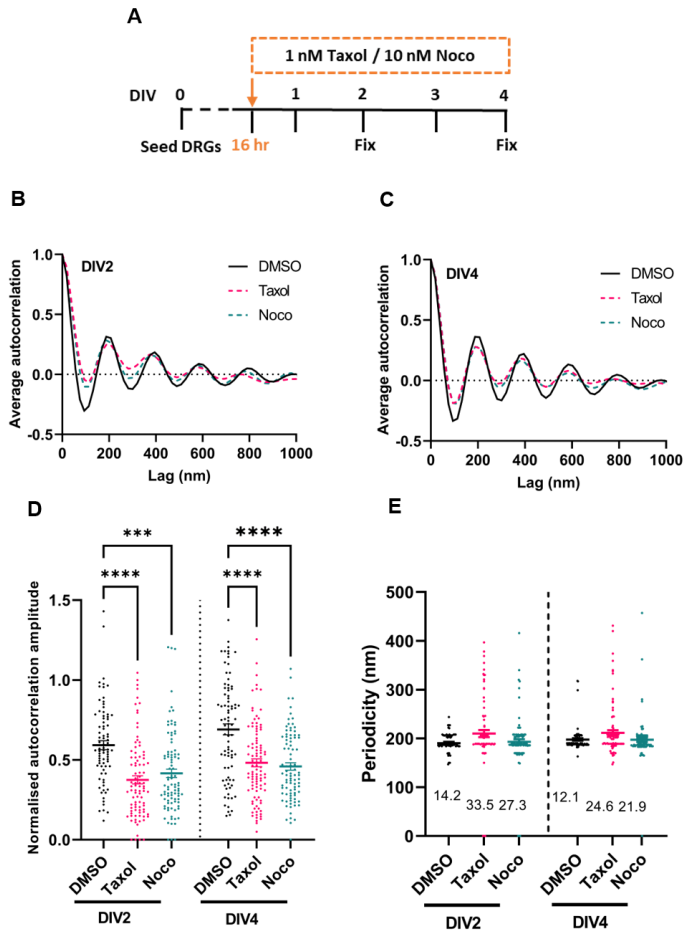

Figure 3: Microtubule dynamics are crucial for MPS formation. (A) Timeline of the experiment. 1 nM Taxol or 10 nM Nocodazole was added 16 hr after seeding the neurons and fixed either after another 32 hrs (DIV2) or after 80 hrs (DIV4). (B,C) Average autocorrelation curves drop for βII-spectrin stained axons from cultures treated with 10 nM Nocodazole (green dotted curve) and 1 nM Taxol (pink dotted curve) compared to DMSO (black curve). (D)The normalised autocorrelation amplitudes of the βII-spectrin rings. The data were analysed using the Brown-Forsythe and Welch ANOVA test with multiple comparisons corrected by Games-Howell's test (***, $p \leq 0.001$; ****, $p \leq 0.0001$). (E) Periodicity across DIVs demonstrates an increase in variability between the βII-spectrin rings. The numbers below each data set indicate the coefficient of variation of the distribution. For B-E, 82-100 axonal segments from 3 biological replicates for each DIV were analysed.

F-actin stabilisation or actomyosin activity does affect axonal MPS development

A recent study in fibroblasts has suggested that acto-myosin contractility may drive spectrin clustering and periodic distribution of βII-spectrin (Ghisleni et al., 2024). Suppression of actin dynamics (treatment with jasplakinolide) increased periodic βII-spectrin clusters via myosin activity, while the inhibition of non-muscle myosin II (by blebbistatin) dissipated the βII-spectrin clusters (Ghisleni et al., 2024).

In axons, however, an acute reduction of F-actin turnover by jasplakinolide (Jasp) did not affect the MPS (Fig. 2). We tested if a chronic, low-dose stabilisation of F-actin would affect MPS development. 10 nM Jasp was added to DRG cultures 16 h post-seeding, and neurons were fixed at DIV2 and DIV4. As reported earlier, Jasp treatment resulted in shorter axons (Gallo et al., 2002), but the development of the βII-spectrin MPS was unaffected at both DIV2 and 4 (Fig. 4) compared to vehicle

treatment. Curiously, the axons chronically exposed to Jasp were substantially thicker compared to the controls, and this was reflected in the increased βII-spectrin ring diameter (Fig. S3C). The diameter of the βII-spectrin rings did not change in response to acute treatment with Jasp as described earlier (Fig. S2), and it appears to be specific to long-term exposure and not dependent on the absence of the βII-spectrin MPS. In addition to stabilising F-actin, Jasp can also nucleate F-actin under certain conditions (Bubb et al., 2000). Chronic exposure to Jasp may lead to excessive, hyperstabilised axonal F-actin that results in short and thick axons. The stronger spectrin signal in Jasp-treated axon compared to controls observed may reflect the latter speculation (Fig. S3D).

Acute inhibition of myosin activity has been previously shown to increase axonal and βII-spectrin ring diameter without affecting the periodic organisation of the MPS (Costa et al., 2020; Wang et al., 2020; Zhou et al., 2022). We again developed a low-dose, chronic exposure protocol with 10 μM blebbistatin (Bleb) added to DRG cultures 16 h post-seeding and the neurons fixed for analysis at DIV2 and DIV4. Low-dose, prolonged inhibition of non-muscle myosin II did affect the development of the βII-spectrin MPS (Fig. 4). However, consistent with the involvement of myosin contractility in maintaining axonal diameter (Costa et al., 2020; Wang et al., 2020), treatment with a low concentration of Bleb increased the average diameter of βII-spectrin rings compared to controls (Fig. S3C).

Our data suggest that, unlike in fibroblasts, actomyosin activity does not drive the assembly of periodic βII-spectrin clusters in axons.

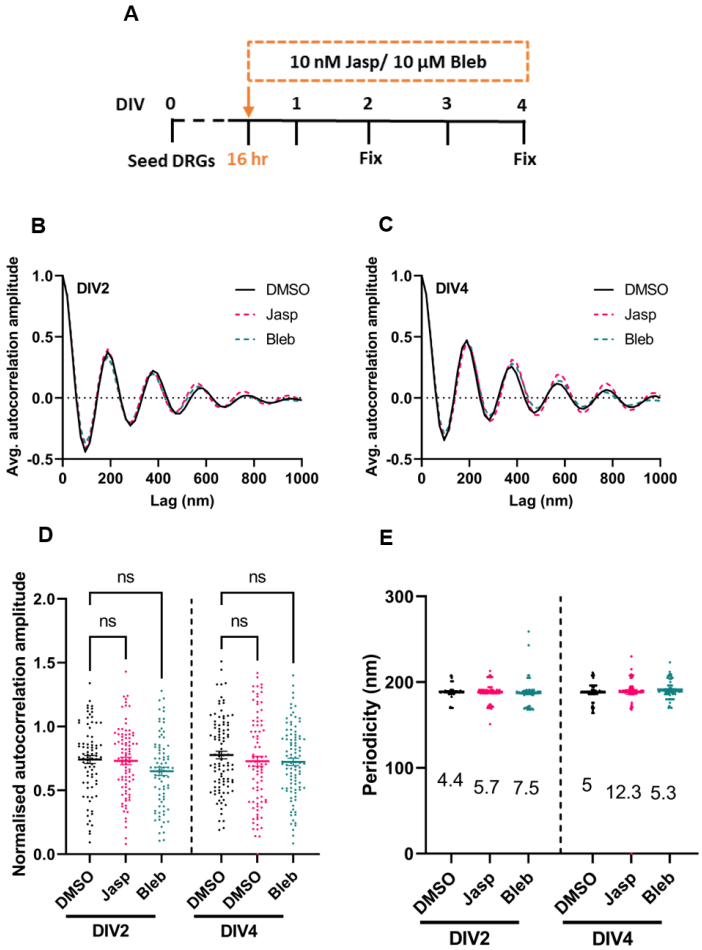

Figure 4: Actin stabilisation or myosin contractility does not affect MPS formation. (A) Timeline of the experiment. 10 nM Jasplakinolide or 10 μM Blebbistatin was added 16 hr after seeding the neurons and fixed either after another 32 hrs (DIV2) or after 80 hrs (DIV4). (B, C) Average autocorrelation curves show no difference for βII- spectrin stained axons from cultures treated with 10 μM Blebbistatin (green dotted curve) and 10 nM Jasplakinolide (pink dotted curve) compared to DMSO (black curve). (D)The normalised autocorrelation amplitudes of the βII-spectrin rings. The data were analysed using the Brown-Forsythe and Welch ANOVA test with multiple comparisons corrected by Games-Howell's test (ns, $p > 0.05$). (E) Periodicity across DIVs demonstrates variability between the βII-spectrin rings. The numbers below each data set indicate the coefficient of variation of the distribution. For B-E, 79-98 axonal segments from 3 biological replicates for each DIV were analysed.

Actin nucleators Arp2/3 and Formins regulate MPS development in the early but not late stages

F-actin structures in cells are initiated by the activity of actin nucleators, which also modulate the morphology and dynamics of these structures. Previous reports indicate that MPS formation is impaired in neurons derived from *Drosophila* carrying loss-of-function mutations in the actin nucleators Arp2/3 and the formin DAAM (Qu et al., 2017). Given the dependence of the βII-spectrin MPS on F-actin (Fig. 2), we investigated the contribution of Arp2/3 and formins in MPS organisation at different developmental time points.

We exposed DRG neurons at different DIVs to the Arp2/3 complex inhibitor, CK666 (20 μM for 30 mins) or the formin inhibitor, SMIFH2 (20 μM for 30 mins). Inhibition of Arp2/3 or the formins in early-stage neurons (DIV2 and DIV4) led to the disorganisation of the βII-spectrin MPS with decreased autocorrelation and average autocorrelation amplitudes (Fig. 5A-C). These were accompanied by an increase in the variability of the MPS spacing, though the mean values were not statistically different. However, at DIV 6, inhibition of neither the Arp2/3 complex nor formin activity disrupted the abundance or periodicity of the MPS. These results suggest that MPS development requires both the linear (formins) and branched nucleators (Arp2/3) at the early developmental stages; however, actin nucleation is dispensable for the maintenance of stable MPS.

The formin inhibitor, SMIFH2, also inhibits myosin II at high doses (Nishimura et al., 2021). As inhibition of myosin II increases the axonal diameter (Costa et al., 2020; Wang et al., 2020), we tested if treatment with SMIFH2 altered axonal diameter at DIV6 (no effect on MPS organisation at this stage). No change in the diameter of the βII-spectrin ring was observed following SMIFH2 treatment of DIV6 neurons (Fig S5), suggesting that the dose used in our experiments does not inhibit myosin II significantly. However, the compromised periodic organisation of βII-spectrin observed in early DIV2 and 4 upon treatment with either SMIFH2 or CK666 resulted in increased βII-spectrin ring diameter only at DIV2 and DIV4 but not at DIV6 (Fig. S5).

F-actin is necessary to crosslink multiple spectrin heterotetramers to form the mature axially concatenated arrangement of alternating F-actin rings and spectrins. In addition, the recruitment and retention of spectrin heterotetramers to the axonal cortex, prior to the development of a strongly periodic scaffold, could depend on subplasmalemmal F-actin. Our data indicating the sensitivity of the earlier stages to the inhibition of F-actin nucleation suggest labile F-actin structures with faster F-actin turnover at these stages. However, at later stages (DIV6), F-actin structures are more stable with reduced dependency on fresh nucleation and/or formin-dependent filament elongation.

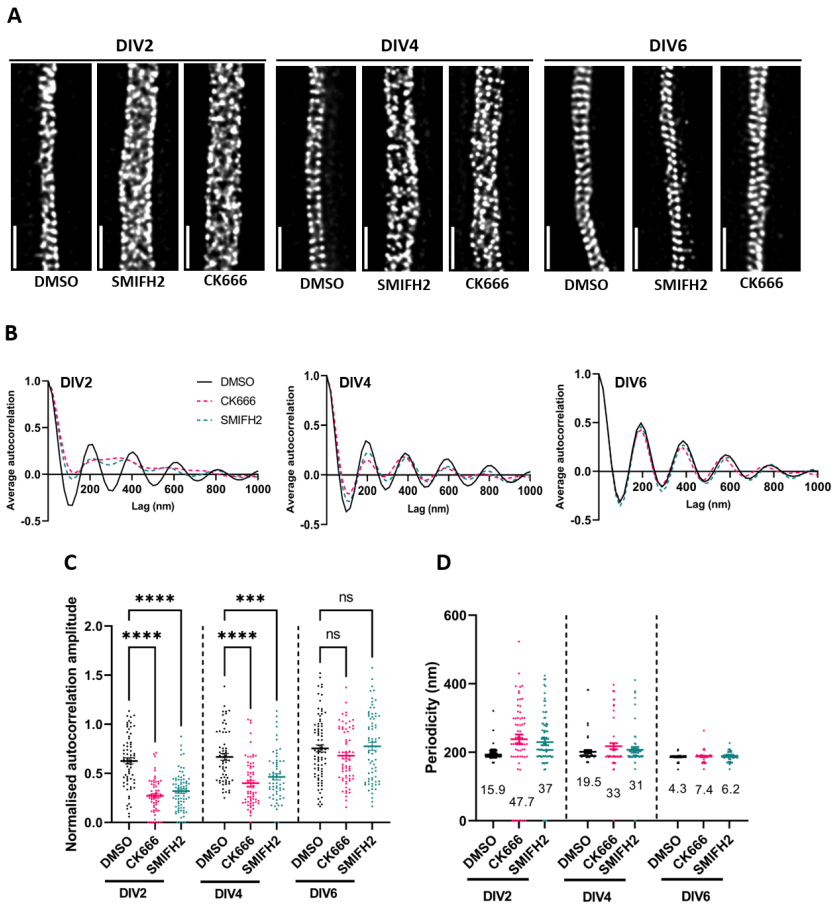

Figure 5: Formins and Arp2/3 affect MPS formation and maintenance. (A) Representative micrographs of single optical sections from STED nanoscopy of DIV2, DIV4, and DIV6 DRG axons stained with βII-spectrin post-treatment with DMSO control, Formin inhibitor (SMIFH2; 20 µM, 30 min) or Arp2/3 inhibitor (CK666; 20 µM, 30 min). Scale bar: 1 µm (B) Average autocorrelation curves across multiple axonal regions for all treatments. (C) The normalised autocorrelation amplitudes of the βII- spectrin rings. The data were analysed using the Brown-Forsythe and Welch ANOVA test with multiple comparisons corrected by Games -Howell's test (ns, $p > 0.05$; ***, $p \leq 0.001$, ****, $p \leq 0.0001$) (D) Periodicity across DIVs demonstrates an increase in variability between the βII-spectrin rings at DIV2 and 4. The numbers below each data set indicate the coefficient of variation of the distribution. For B-D, 60-70 axonal segments from 3 biological replicates for each DIV were analysed.

βII-spectrin progressively associates with the axonal cortex via interactions with F-actin

As the axon develops, βII-spectrin is recruited to the cellular cortex and progressively evolves into a highly periodic organisation (Fig. 1). We find early subplasmalemmal recruitment of βII-spectrin by DIV1 (Fig. 1A-D) and a dependence on F-actin (Figs. 2 and 5) in initiating MPS formation. To evaluate the dynamics of subplasmalemmal βII-spectrin, we employed fluorescence recovery after photobleaching (FRAP) analysis of DRG neurons transfected with GFP-tagged βII spectrin (βII-spectrin-GFP) at different developmental stages (Fig. 6A). To exclude cytoplasmic spectrin resulting from overexpression, only axons with low expression of βII spectrin-GFP were selected for the analysis.

Analysis of the normalised recovery curves and the mobile fraction, demonstrated a gradual decrease in the overall mobility of βII-spectrin, with a marked reduction as

531 development progresses from DIV1 to DIV4 (Fig. 6A,B). The half-life ($t_{1/2}$) of the
532 recovery was similar across DIVs, indicating no change in the rate of diffusion of βII-
533 spectrin (Fig. 6C). These data are consistent with the increase in the autocorrelation
534 amplitude from DIV1 to DIV4 (Fig. 1), indicating that the βII-spectrin scaffold
535 becomes increasingly stable with development. However, even at the early stages
536 (DIV1), the mobile fraction is under 50%. This suggests that βII-spectrin is already
537 recruited to the axonal cortex by DIV1 with restricted mobility.

538 Recruitment of spectrin heterotetramers to the cortex may involve interactions with
539 the cortical F-actin. The sensitivity to F-actin deregulation observed earlier (Figs. 2
540 and 5) likely reflects this association. To explore the role of F-actin in βII-spectrin
541 mobility, we treated βII-spectrin-GFP transfected DIV1, 2, and 4 DRG neurons with 5
542 μM Lat-A for 15 min (same dose as that used in the data represented in Fig. 2)
543 before FRAP analysis. In contrast to the DMSO-treated control recovery curves for
544 DIV1 and DIV2 neurons, the Lat-A-treated axons exhibited increased βII-spectrin
545 mobility with an elevated mobile fraction (Fig. 6D-E). However, the recovery kinetics
546 of βII-spectrin-GFP in DIV4 axons treated with Lat-A were comparable to DMSO-
547 treated controls. In all cases, there was no change in the $t_{1/2}$ of the recovery (Fig.
548 6F).

549 These data suggest that a significant proportion of βII-spectrin is associated with the
550 axonal cortex as early as DIV1 and constitutes a stable spectrin pool. A major
551 component of this early association is via interactions with subplasmalemmal F-actin,
552 though this dependence is reduced by DIV 4, perhaps due to the recruitment of other
553 interactions that stabilise the association or increased resistance of mature cortical
554 F-actin to depolymerisation. The increased stability of βII-spectrin correlates with the
555 progressive establishment of long-range, periodic order of the MPS with
556 developmental time (Fig. 1).

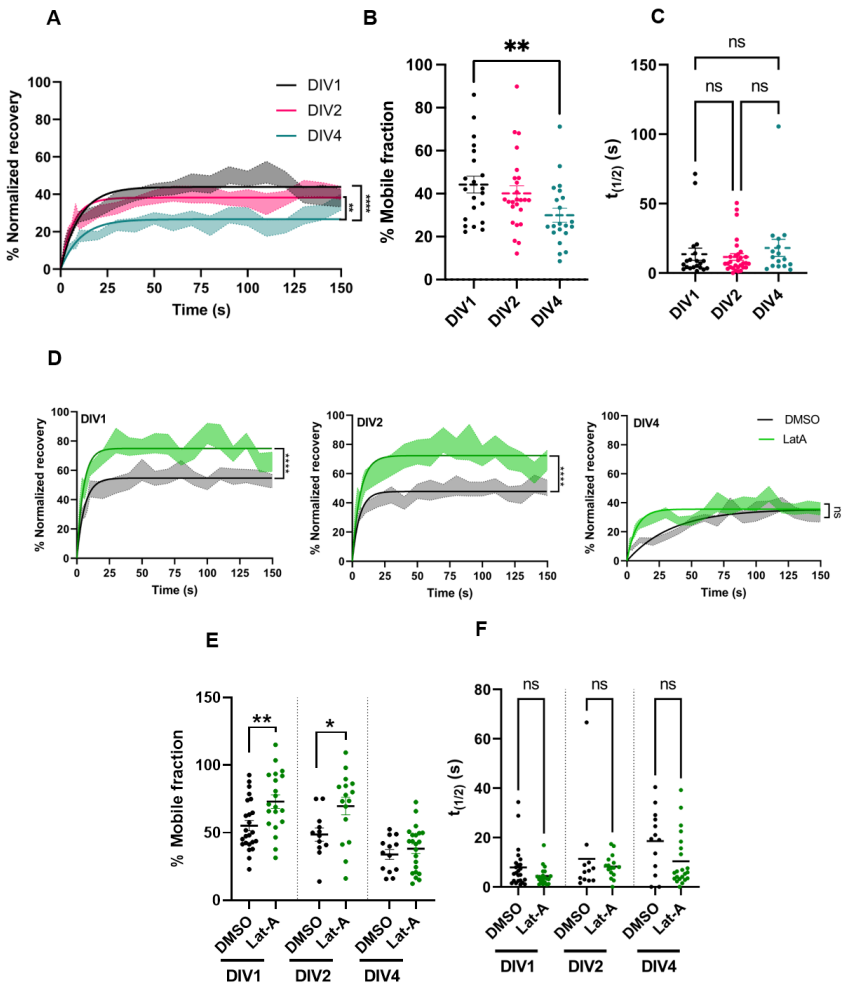

557

558 **Figure 6: Spectrin mobility is correlated with MPS maturation and dependent on F-actin-**
559 **mediated cortical recruitment.** (A) βII-spectrin-GFP FRAP recovery curves for the DIV1, DIV2, and
560 DIV4 axons. The recovery curves are represented as a one-phase fit of the means (± SEM). Plateau
561 of curves were compared using the extra sum-of-squares F-test. (B) Quantification of the % mobile
562 fraction. The data were analysed using the Mann-Whitney test. (C) *t1/2* values of recovery curves
563 obtained from one-phase fit of Latrunculin A and DMSO-treated DRG neurons. Data were analysed
564 using the Kruskal-Wallis test. For A-C, 16-30 neurons for all DIVs from 3 biological replicates were
565 analysed (D) βII-spectrin-GFP FRAP recovery curves for DRG axons treated with Lat-A across DIV1,
566 DIV2 and DIV4. The green and black traces represent the average one-phase fit for Lat-A- and
567 DMSO-treated neurons, respectively. The recovery curves are represented as a one-phase fit of the
568 means (± SEM). Plateau of curves were compared using the extra sum-of-squares F-test. (E)
569 Quantification of the % mobile fraction. The data were analysed using the Mann-Whitney test. In this
570 experiment, 12-24 neurons for all DIVs from 3 biological replicates were analysed. (F) *t1/2* values of
571 recovery curves obtained from one-phase fit of Latrunculin A and DMSO-treated DRG neurons. Data
572 were analysed using the Kruskal-Wallis test. 12-24 neurons for all DIVs from 3 biological replicates
573 were analysed. (ns, $p > 0.05$; *, $p \leq 0.05$; **, $p \leq 0.01$).

574

575 **F-actin and membrane interactions recruit βII spectrin to the axonal cortex for**
576 **MPS development**

577 βII-spectrin is recruited to and stably associates with the axonal cortex early in
578 development (Fig. 6). To examine how early recruitment influences MPS
579 development and dissect the underlying mechanisms, we developed differentiated
580 SH-SY5Y human neuroblastoma cells as a model. Using a differentiation protocol
581 (see Methods) involving sequential treatment with retinoic acid (RA) and brain-

582 derived neurotrophic factor (BDNF), we characterised the development of the βII-
583 spectrin MPS in the axon-like SH-SY5Y neurites (Fig. 7A). βII-spectrin
584 autocorrelation and the autocorrelation amplitude both increased following BDNF
585 treatment for 4, 6 and 8 days (Fig. 7B-D). The periodicity measurements
586 demonstrated a progressive decrease in the MPS spacing variability, reaching 191 ±
587 3.17 nm after 8 days (Fig. 7E), indicating a developmental pattern comparable to
588 DRG neurons (Fig. 1). Next, we generated βII-Spectrin knockout SH-SY5Y cells (βII-
589 Spectrin KO) using CRISPR-Cas9 technology and verified the knockout through
590 genomic sequencing (Fig. S7 A,B) and immunoblotting (Fig. 7 F). As expected, the
591 βII-Spectrin-KO SH-SY5Y neurons displayed reduced axonal lengths (Fig. S7C,D),
592 consistent with the phenotype reported for neurons derived from βII-Spectrin
593 knockout mice (Lorenzo et al., 2019).

594 To parse the contributions from various βII-spectrin interactions, we generated
595 variants of βII-spectrin fused with green fluorescent protein (GFP; Fig. 8A). These
596 included the full-length human βII-Spectrin protein, as well as mutants lacking
597 ankyrin B binding (βII-Spectrin-Y1874A), plasma membrane recruitment via the PH
598 domain (βII-Spectrin-K2207Q), and actin-binding (βII-Spectrin-ΔABD). We imaged
599 GFP-labelled axons using STED nanoscopy 6 days after the transfection of these
600 constructs in the βII-Spectrin knockout SH-SY5Y cells (Fig. 8A). The full-length βII-
601 spectrin and ankyrin B binding deficient protein (βII-Spectrin-Y1874A) were recruited
602 to the axonal cortex and formed a periodic scaffold (Fig. 8B-D). However, both the
603 PH domain (βII-Spectrin-K2207Q) and actin-binding domain (βII-Spectrin-ΔABD)
604 mutants were unable to form a strongly periodic MPS, as quantified by the average
605 autocorrelation curves and autocorrelation amplitudes (Fig. 8B-D). Additionally,
606 periodicity analysis showed a higher coefficient of variation for both these mutants
607 compared to the full-length control (Fig. 8E). These findings demonstrate βII-spectrin
608 recruitment to the subplasmalemmal cortex via actin-binding and membrane
609 interactions of the PH-domain to form the MPS.

610 To investigate the subplasmalemmal recruitment of βII-spectrin further, we
611 performed FRAP analysis of βII-Spectrin KO cells following transfection with different
612 βII-Spectrin mutants. The recovery kinetics of ankyrin B -binding deficient protein
613 (βII-Spectrin-Y1874A) were comparable to the full-length protein (Fig. 9A,B),
614 suggesting that ankyrin B binding is dispensable at these early stages. However, βII-
615 Spectrin deficient in F-actin binding (βII-Spectrin-ΔABD) had a significantly higher
616 mobile fraction and reduced $t_{1/2}$ indicating compromised recruitment to the axonal
617 cortex (Fig. 9A,B). This observation is consistent with the elevated mobile fraction of
618 βII-Spectrin observed upon F-actin disruption by Lat-A treatment in primary DRG
619 neurons (Fig. 6D,E).

620 The mobile fraction estimated from the recovery curves of the PH domain mutant
621 (βII-Spectrin-K2207Q) was comparable to the wild-type protein (Fig. 9A,B). However,
622 the $t_{1/2}$ of the recovery was significantly reduced (Fig. 9C). This suggests no change
623 in the proportion of bound βII-Spectrin-K2207Q molecules but a higher diffusion rate.
624 Given that transfection of βII-Spectrin-K2207Q results in compromised recovery of
625 the MPS (Fig. 8 B-E), this implicates βII-Spectrin PH domain interactions in
626 constraining the kinetics of βII-Spectrin and, in turn, its recruitment to the cortical
627 scaffold.

628 Collectively, these data identify βII-Spectrin interactions with F-actin and the plasma
629 membrane for early recruitment and stabilisation of βII-Spectrin at the axonal cortex
630 as a necessary prerequisite for MPS development.

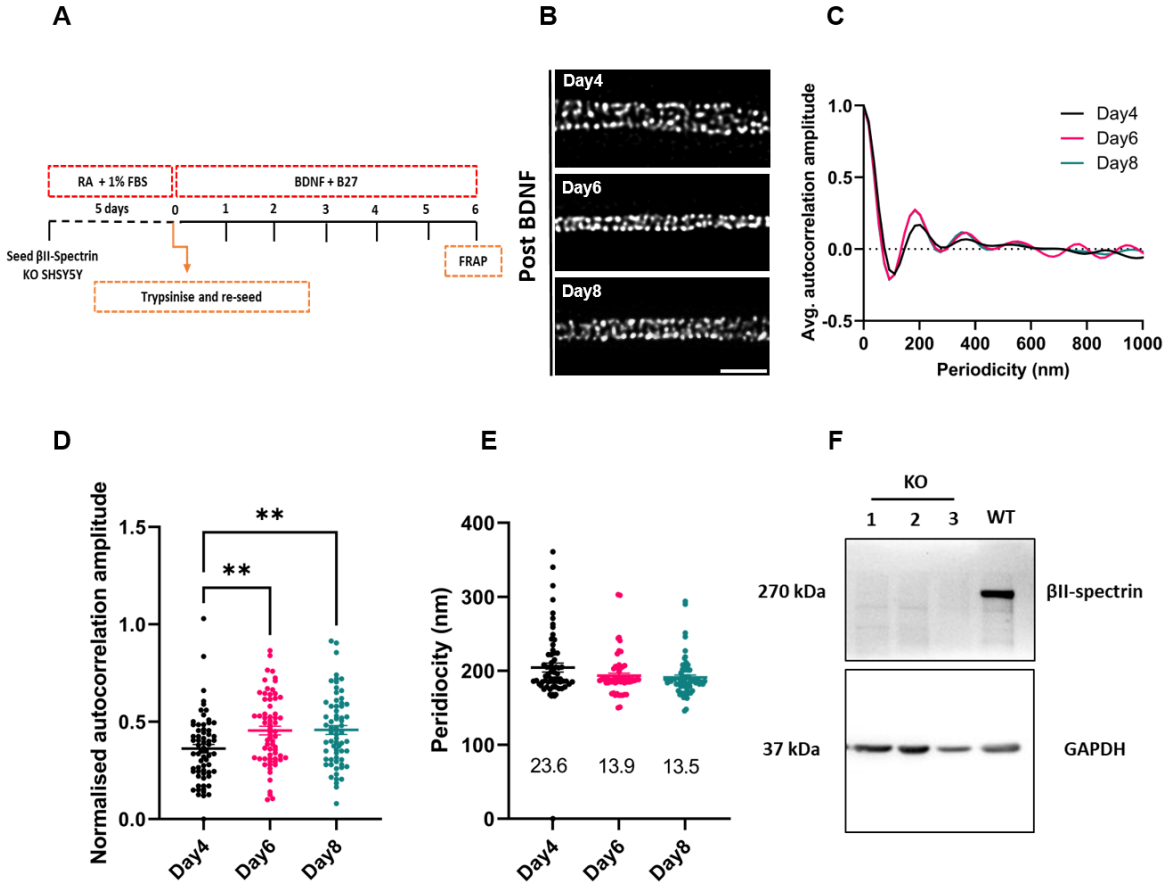

631

632 **Figure 7: MPS in differentiated SH-SY5Y neurons. (A) Timeline indicating the differentiation**
633 **protocol of SH-SY5Y cells.** (B) Representative micrographs of single optical sections from STED
634 nanoscopy of βII-spectrin stained differentiating neurons (4, 6, and 8 days post-BDNF). Scale bar: 1
635 µm. (C, D) Average autocorrelation curves and quantification of normalised autocorrelation
636 amplitudes across time points. The data were analysed using the Brown-Forsythe and Welch ANOVA
637 test with multiple comparisons corrected by Games-Howell's test. (**, $p \leq 0.01$). (E) Periodicity across
638 days demonstrates a reduction in variability. The numbers below each data set indicate the coefficient
639 of variation of the distribution. For B-E, 65 axonal segments from 3 biological replicates for each time-
640 point were analysed. (F) Immunoblot validating the CRISPR-Cas9-based generation of βII-spectrin
641 knockout line in SH-SY5Y cells (βII-Spectrin KO). KO-1 was used for all subsequent analyses.

642

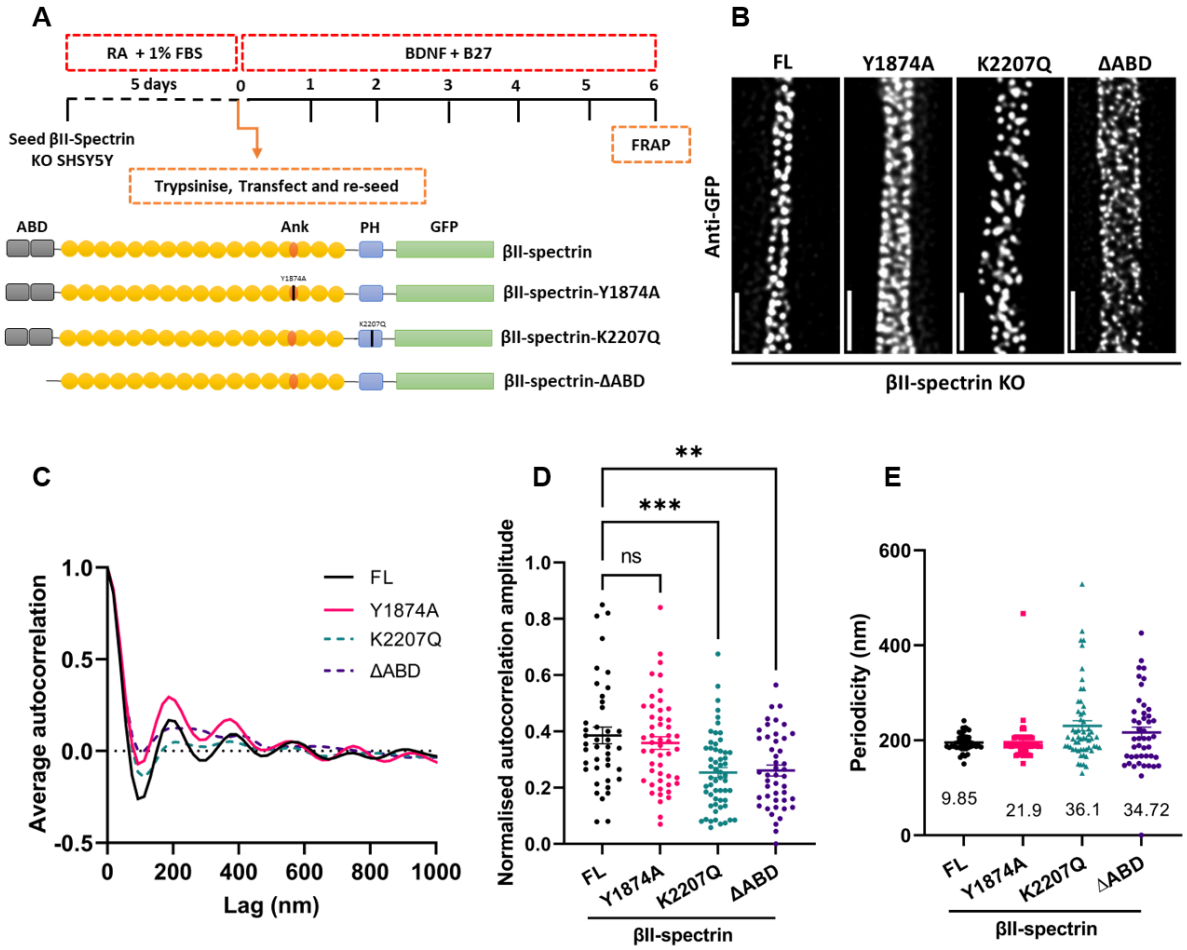

Figure 8: Actin-binding and plasma membrane interactions of βII-spectrin are necessary for MPS development. (A) Timeline indicating the differentiation protocol of βII-Spectrin KO cells and experimental procedures. βII-spectrin KO were transfected mid-differentiation with βII-spectrin variants indicated. The domains are denoted as follows: GFP-tag in green, actin-binding domain (ABD) in grey, ankyrin domain-binding domain in orange, and plasma membrane-binding domain in blue. (B) Representative micrographs of single optical sections from STED nanoscopy of anti-GFP stained differentiated neurites (day 6 post-BDNF) transfected with βII-spectrin variants. (C) Average autocorrelation curves and quantification of normalised autocorrelation amplitudes for all βII-spectrin variants. The data were analysed using the Brown-Forsythe and Welch ANOVA test with multiple comparisons corrected by Games-Howell's test. (E) Periodicity analysis demonstrates high variation in the spacing between the βII-spectrin rings in K227Q and ΔABD variants. The numbers below each data set indicate the coefficient of variation of the distribution. In this experiment, 40–60 axonal regions were examined for each condition across 3 biological replicates. (ns, $p > 0.05$; **, $p \leq 0.01$; ***, $p \leq 0.001$).

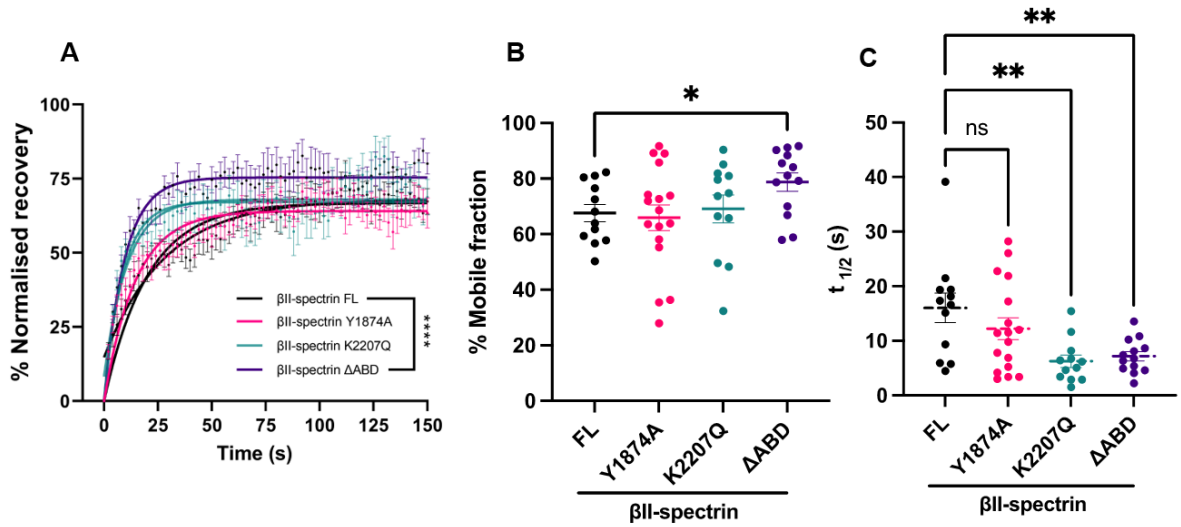

Figure 9: Actin-binding and membrane interactions drive βII-spectrin recruitment and mobility. (A) FRAP recovery curves of mutant and βII-FL-spectrin expressing βII-Spectrin KO cells 6 days after transfection and BDNF treatment. The recovery curves are represented as a one-phase fit of the means (± SEM). Plateau of curves were compared using the extra sum-of-squares F-test. (B) Quantification of the % mobile fraction. The data were analysed using the Mann-Whitney test. (C) t1/2 values extracted from the fit were analysed using the one-way ANOVA test. In this experiment, 12-17 neurons for all DIVs from 3 biological replicates were analysed (ns, $p > 0.05$; *, $p \leq 0.05$; **, $p \leq 0.01$; ****, $p \leq 0.0001$).

668 **DISCUSSION**

669 Spectrin heterotetramer-based subplasmalemmal scaffolds are common across cell
670 types (Ghisleni et al., 2020; Leterrier and Pullarkat, 2022) but form a unique periodic
671 structure with long-range order in neuronal axons. Given the myriad functions
672 ascribed to the axonal MPS (Albrecht et al., 2016; Lorenzo et al., 2019; Zhou et al.,
673 2019, 2022; Costa et al., 2020), there is considerable interest in understanding the
674 early development of the axonal MPS. Here, we focus on embryonic DRG neurons
675 to uncover the cytoskeleton-mediated mechanisms underlying the recruitment of
676 spectrin to the axonal cortex, the maturation of the βII-Spectrin scaffold to a lattice-
677 like periodic organisation and the maintenance of the MPS.

678 In this study, we evaluate the medial axonal segments of DRG axons to investigate
679 the establishment of long-range periodic order and the typical spacing of the βII-
680 Spectrin MPS. We find that βII-Spectrin is already present at the axonal cortex by
681 DIV1, though its organisation is weakly periodic. The scaffold matures progressively
682 with development, with the degree of periodicity increasing and the variability of the
683 spectrin spacing concomitantly decreasing and converging to ~185 nm by DIV 6 (Fig
684 1A-E). However, there is no obvious change in the amount of βII-Spectrin (Fig S1A)
685 between DIVs indicating re-modelling of early recruited spectrin to a periodic
686 organisation with long-range order. These data also indicate a more rapid
687 development of the MPS in embryonic DRG neurons compared to hippocampal
688 (Zhong et al., 2014) and cortical neurons (Hofmann et al., 2022).

689 The progressive maturation of the MPS was coincident with a reduction in the axonal
690 diameter. The role of the MPS in regulating axonal diameter has been demonstrated
691 previously (Costa et al., 2020; Wang et al., 2020), and our data suggests maturation
692 of the MPS results in increased radial constriction, possibly due to the increased
693 recruitment of myosin and stabilisation of the F-actin rings. Our data suggest that the
694 corseting of the axon shaft by the MPS regulates axon diameter, and all
695 manipulations that disrupt the MPS result in increased βII-Spectrin ring diameter.
696 These data not only support the correspondence between long-range, periodic MPS
697 and axonal morphology but also indicate that the MPS provides both passive and
698 active (via actomyosin contractility) regulation of the axonal diameter.

699 Axonal pre-tension also increases modestly with the increase in the periodic
700 organisation, though it is interesting to note that even at DIV1 there is substantial
701 pre-tension. Axonal pre-tension has been previously associated with spectrin (Krieg
702 et al., 2014), and the non-periodic organisation of spectrin in non-neuronal cells are
703 also load-bearing (Lee and Discher, 2001; Smith et al., 2018; Ghisleni et al., 2020).
704 The weakly periodic spectrin organisation observed at DIV1 may form a networked
705 scaffold that supports the axonal pre-stress. However, cytoskeletal components are
706 also likely to contribute significantly as load-bearing structures in the axon (Mutalik et
707 al., 2018; Leterrier and Pullarkat, 2022; Ghose and Pullarkat, 2023).

708 Acute depolymerisation of microtubules led to the destabilisation of the MPS at all
709 developmental stages (Fig. 2). This suggests a microtubule-dependent MPS
710 maintenance function. Similar observations have been made in hippocampal
711 neurons (Zhong et al., 2014). Conversely, in *Drosophila* neurons, periodic actin is
712 proposed to maintain microtubule alignment and stability (Qu et al., 2017). In *C.*
713 *elegans*, loss of spectrin reduces the length of axonal microtubules in some neurons
714 (Krieg et al., 2017). To probe the contribution of microtubule to MPS formation
715 further, we subjected early axons to a low chronic dose of microtubule modifying

716 drugs (Fig. 3). As with the acute treatment, continuous exposure to a low dose of
717 Noco from 16h after seeding, resulted in compromised MPS in both DIV 2 and DIV4.
718 Surprisingly, and in contrast to acute treatment with Taxol, chronic stabilisation of
719 microtubules in early axons also destabilised the MPS at both DIV 2 and 4. These
720 observations suggest the requirement of microtubule dynamics in the establishment
721 of the βII-Spectrin MPS. Apart from stabilising microtubules, Taxol can also promote
722 microtubule growth and nucleation, these changes may influence MPS development
723 (Witte et al., 2008; Verma et al., 2016). In epithelial lateral membranes, the mobility
724 of spectrin domains is sensitive to microtubule depolymerisation (Jenkins et al.,
725 2015), however, it is unclear if an analogous or distinct mechanism is involved in
726 axonal MPS development. Recent *in vivo* studies in *C. elegans* suggest a balance
727 between spectrin transport and assembly (Glomb et al., 2023). Though chronic
728 treatment with Noco or Taxol resulted in compromised MPS without any changes in
729 axonal βII-Spectrin intensity, subtle deficits in transport are likely to be unresolved
730 due to the high abundance of relatively stationary spectrin.

731 Acute depolymerisation but not stabilisation of F-actin resulted in the loss of βII-
732 spectrin MPS across all stages of early development as has also been demonstrated
733 in both young and older axons (Zhong et al., 2014; Han et al., 2017; Qu et al., 2017).
734 A key role of F-actin, in the form of the circumferential rings, involves the crosslinking
735 of spectrin heterotetramers into the longitudinal periodic arrangement seen in axons
736 (Xu et al., 2013; Vassilopoulos et al., 2019). Further, subplasmalemmal F-actin is
737 likely to facilitate the cortical recruitment of spectrin heterotetramers early in
738 development and initiate the organisation of the crosslinked spectrin scaffold.
739 Inhibition of actin nucleation early in development (DIV2, 4) resulted in disruption of
740 the MPS. However, acute inhibition of actin nucleation at later stages (DIV 6) did not
741 affect the established MPS. This suggests that dynamically nucleating actin networks
742 in early development are required for MPS development, but the contribution of fresh
743 actin nucleation-dependent turnover, over the timescales evaluated, is not necessary
744 for MPS maintenance.

745 FRAP experiments revealed that βII-spectrin gets increasingly stabilised at the
746 axonal cortex with development, consistent with previous observations in
747 hippocampal neurons (Xu et al., 2013). We show that a significant component of the
748 cortical recruitment of βII-spectrin is via interactions with F-actin, though this
749 dependency reduces as the MPS matures. As βII-spectrin but not αII-spectrin can
750 directly bind F-actin (Li and Bennett, 1996) , the latter is expected to drive the
751 interactions of the spectrin heterotetramer with cortical actin.

752 To further probe subplasmalemmal recruitment of βII-spectrin, we developed a
753 model of differentiated human SH-SY5Y cells engineered to lack βII-spectrin. By
754 expressing βII-spectrin spectrin variants in this system, we established the essential
755 roles of the membrane-interacting PH domain and the actin-binding domain in the
756 development of the MPS. These data are consistent with observations in mouse
757 neurons (Zhou et al., 2022). FRAP analysis of mutant spectrin revealed that the
758 actin-binding domain of βII-spectrin is required for its recruitment and stabilisation at
759 the axonal cortex. Additionally, interactions with the plasma membrane lipids via the
760 PH domain also contribute to subplasmalemmal confinement.

761 In fibroblasts, actomyosin activity can drive the transition from a diffuse orientation of
762 βII-spectrin to a periodic, clustered configuration (Ghisleni et al., 2024). In contrast,
763 blebbistatin treatment does not affect the MPS organisation in mature neurons,

764 though it increases the axonal diameter by reducing radial contractility (Costa et al.,
765 2020; Wang et al., 2020). However, as early DRG axons are actively contractile
766 (Mutalik et al., 2018), there may be a role for actomyosin contractility in driving the
767 reorganisation of βII-spectrin to a periodic scaffold. Early and chronic inhibition of
768 myosin did not affect axonal MPS formation while increasing the axonal diameter.
769 These data suggest that, unlike in fibroblasts, actomyosin contractility is dispensable
770 for axonal βII-Spectrin MPS development, perhaps due to differences in topological
771 and mechanical constraints.

772 Recent work has suggested a regulatory coupling between spectrin transport and
773 MPS assembly (Glomb et al., 2023), and there are observations indicative of
774 intercalated MPS assembly in the distal axon (Hofmann et al., 2022; Boyer et al.,
775 2024). Our study focusses on the medial axonal segments and evaluates the
776 developmental remodelling of βII-Spectrin after subplasmalemmal recruitment.
777 Mechanisms identified here are likely to be equally relevant for the distal ends of
778 long axons following cortical recruitment of βII-Spectrin.

779 This study highlights the dynamic remodelling and maturation of the βII-spectrin
780 MPS in early development and identifies stage-specific cytoskeletal contributions.
781 Dynamics of the microtubule and the actin cytoskeletons contribute to the
782 development of the MPS. Interactions with F-actin and the membrane drive the early
783 subplasmalemmal confinement of βII-spectrin, which subsequently matures to an
784 extended scaffold with long-range periodic order and whose maintenance is
785 dependent on both stable F-actin and microtubules.

786

787 **REFERENCES**

788 Albrecht, D., C.M. Winterflood, M. Sadeghi, T. Tschager, F. Noé, and H. Ewers.
789 2016. Nanoscopic compartmentalization of membrane protein motion at the axon
790 initial segment. *J. Cell Biol.* 215:37–46. doi:10.1083/jcb.201603108.

791 Boyer, N.P., R. Sharma, T. Wiesner, A. Delamare, F. Pelletier, C. Leterrier, and S.
792 Roy. 2024. Spectrin condensates provide a nidus for assembling the periodic
793 axonal structure. 2024.06.05.597638. doi:10.1101/2024.06.05.597638.

794 Bubb, M.R., I. Spector, B.B. Beyer, and K.M. Fosen. 2000. Effects of Jasplakinolide
795 on the Kinetics of Actin Polymerization: AN EXPLANATION FOR CERTAIN IN
796 VIVO OBSERVATIONS*. *J. Biol. Chem.* 275:5163–5170.
797 doi:10.1074/jbc.275.7.5163.

798 Costa, A.R., S.C. Sousa, R. Pinto-Costa, J.C. Mateus, C.D. Lopes, A.C. Costa, D.
799 Rosa, D. Machado, L. Pajuelo, X. Wang, F. Zhou, A.J. Pereira, P. Sampaio, B.Y.
800 Rubinstein, I.M. Pinto, M. Lampe, P. Aguiar, and M.M. Sousa. 2020. The
801 membrane periodic skeleton is an actomyosin network that regulates axonal
802 diameter and conduction. *eLife*. doi:10.7554/eLife.55471.

803 Cousin, M.A., B.A. Creighton, K.A. Breau, R.C. Spillmann, E. Torti, S. Dontu, S.
804 Tripathi, D. Ajit, R.J. Edwards, S. Afriyie, J.C. Bay, K.M. Harper, A.A. Beltran, L.J.
805 Munoz, L. Falcon Rodriguez, M.C. Stankewich, R.E. Person, Y. Si, E.A. Normand,
806 A. Blevins, A.S. May, L. Bier, V. Aggarwal, G.M.S. Mancini, M.A. van Slegtenhorst,
807 K. Cremer, J. Becker, H. Engels, S. Aretz, J.J. MacKenzie, E. Brilstra, K.L.I. van
808 Gassen, R.H. van Jaarsveld, R. Oegema, G.M. Parsons, P. Mark, I. Helbig, S.E.
809 McKeown, R. Stratton, B. Cogne, B. Isidor, P. Cacheiro, D. Smedley, H.V. Firth, T.
810 Bierhals, K. Kloth, D. Weiss, C. Fairley, J.T. Shieh, A. Kritzer, P. Jayakar, E. Kurtz-
811 Nelson, R.A. Bernier, T. Wang, E.E. Eichler, I.M.B.H. van de Laar, A. McConkie-
812 Rosell, M.T. McDonald, J. Kemppainen, B.C. Lanpher, L.E. Schultz-Rogers, L.B.
813 Gunderson, P.N. Pichurin, G. Yoon, M. Zech, R. Jech, J. Winkelmann, A.S. Beltran,
814 M.T. Zimmermann, B. Temple, S.S. Moy, E.W. Klee, Q.K.-G. Tan, and D.N.
815 Lorenzo. 2021. Pathogenic SPTBN1 variants cause an autosomal dominant
816 neurodevelopmental syndrome. *Nat. Genet.* 53:1006–1021. doi:10.1038/s41588-
817 021-00886-z.

818 D'Este, E., D. Kamin, C. Velte, F. Göttfert, M. Simons, and S.W. Hell. 2016.
819 Subcortical cytoskeleton periodicity throughout the nervous system. *Sci. Rep.*
820 6:22741. doi:10.1038/srep22741.

821 Dubey, S., N. Bhembre, S. Bodas, S. Veer, A. Ghose, A. Callan-Jones, and P.
822 Pullarkat. 2020. The axonal actin-spectrin lattice acts as a tension buffering shock
823 absorber. *eLife*. 9:e51772. doi:10.7554/eLife.51772.

824 Gallo, G., H.F. Yee Jr., and P.C. Letourneau. 2002. Actin turnover is required to
825 prevent axon retraction driven by endogenous actomyosin contractility. *J. Cell Biol.*
826 158:1219–1228. doi:10.1083/jcb.200204140.

827 Ghisleni, A., M. Bonilla-Quintana, M. Crestani, Z. Lavagnino, C. Galli, P.
828 Rangamani, and N.C. Gauthier. 2024. Mechanically induced topological transition

829 of spectrin regulates its distribution in the mammalian cell cortex. *Nat. Commun.*
830 15:5711. doi:10.1038/s41467-024-49906-6.

831 Ghisleni, A., C. Galli, P. Monzo, F. Ascione, M.-A. Fardin, G. Scita, Q. Li, P. Maiuri,
832 and N.C. Gauthier. 2020. Complementary mesoscale dynamics of spectrin and
833 acto-myosin shape membrane territories during mechanoresponse. *Nat. Commun.*
834 11:5108. doi:10.1038/s41467-020-18825-7.

835 Ghose, A., and P. Pullarkat. 2023. The role of mechanics in axonal stability and
836 development. *Semin. Cell Dev. Biol.* 140:22–34.
837 doi:10.1016/j.semcdb.2022.06.006.

838 Glomb, O., G. Swaim, P. Munoz LLancao, C. Lovejoy, S. Sutradhar, J. Park, Y. Wu,
839 S.E. Cason, E.L.F. Holzbaur, M. Hammarlund, J. Howard, S.M. Ferguson, M.W.
840 Gramlich, and S. Yogev. 2023. A kinesin-1 adaptor complex controls bimodal slow
841 axonal transport of spectrin in *Caenorhabditis elegans*. *Dev. Cell*. 58:1847-
842 1863.e12. doi:10.1016/j.devcel.2023.08.031.

843 Hammarlund, M., E.M. Jorgensen, and M.J. Bastiani. 2007. Axons break in animals
844 lacking β-spectrin. *J. Cell Biol.* 176:269–275. doi:10.1083/jcb.200611117.

845 Han, B., R. Zhou, C. Xia, and X. Zhuang. 2017. Structural organization of the actin-
846 spectrin–based membrane skeleton in dendrites and soma of neurons. *Proc. Natl.*
847 *Acad. Sci.* 114:E6678–E6685. doi:10.1073/pnas.1705043114.

848 He, J., R. Zhou, Z. Wu, M.A. Carrasco, P.T. Kurshan, J.E. Farley, D.J. Simon, G.
849 Wang, B. Han, J. Hao, E. Heller, M.R. Freeman, K. Shen, T. Maniatis, M. Tessier-
850 Lavigne, and X. Zhuang. 2016. Prevalent presence of periodic actin–spectrin-based
851 membrane skeleton in a broad range of neuronal cell types and animal species.
852 *Proc. Natl. Acad. Sci.* 113:6029–6034. doi:10.1073/pnas.1605707113.

853 Hofmann, M., L. Biller, U. Michel, M. Bähr, and J.C. Koch. 2022. Cytoskeletal
854 assembly in axonal outgrowth and regeneration analyzed on the nanoscale. *Sci.*
855 *Rep.* 12:14387. doi:10.1038/s41598-022-18562-5.

856 Huang, C.Y.-M., C. Zhang, T.S.-Y. Ho, J. Oses-Prieto, A.L. Burlingame, J. Lalonde,
857 J.L. Noebels, C. Leterrier, and M.N. Rasband. 2017a. αII Spectrin Forms a Periodic
858 Cytoskeleton at the Axon Initial Segment and Is Required for Nervous System
859 Function. *J. Neurosci.* 37:11311–11322. doi:10.1523/JNEUROSCI.2112-17.2017.

860 Huang, C.Y.-M., C. Zhang, D.R. Zollinger, C. Leterrier, and M.N. Rasband. 2017b.
861 An αII Spectrin-Based Cytoskeleton Protects Large-Diameter Myelinated Axons
862 from Degeneration. *J. Neurosci.* 37:11323–11334. doi:10.1523/JNEUROSCI.2113-
863 17.2017.

864 Jenkins, P.M., M. He, and V. Bennett. 2015. Dynamic spectrin/ankyrin-G
865 microdomains promote lateral membrane assembly by opposing endocytosis. *Sci.*
866 *Adv.* 1:e1500301. doi:10.1126/sciadv.1500301.

867 Krieg, M., A.R. Dunn, and M.B. Goodman. 2014. Mechanical control of the sense of
868 touch by β-spectrin. *Nat. Cell Biol.* 16:224–233. doi:10.1038/ncb2915.

869 Krieg, M., J. Stühmer, J.G. Cueva, R. Fetter, K. Spilker, D. Cremers, K. Shen, A.R.
870 Dunn, and M.B. Goodman. 2017. Genetic defects in β-spectrin and tau sensitize C.
871 elegans axons to movement-induced damage via torque-tension coupling. *eLife*.
872 6:e20172. doi:10.7554/eLife.20172.

873 Lee, J.C.-M., and D.E. Discher. 2001. Deformation-Enhanced Fluctuations in the
874 Red Cell Skeleton with Theoretical Relations to Elasticity, Connectivity, and
875 Spectrin Unfolding. *Biophys. J.* 81:3178–3192. doi:10.1016/S0006-3495(01)75954-
876 1.

877 Leterrier, C., and P.A. Pullarkat. 2022. Mechanical role of the submembrane
878 spectrin scaffold in red blood cells and neurons. *J. Cell Sci.* 135:jcs259356.
879 doi:10.1242/jcs.259356.

880 Li, X., and V. Bennett. 1996. Identification of the Spectrin Subunit and Domains
881 Required for Formation of Spectrin/Adducin/Actin Complexes *. *J. Biol. Chem.*
882 271:15695–15702. doi:10.1074/jbc.271.26.15695.

883 Lorenzo, D.N., A. Badea, R. Zhou, P.J. Mohler, X. Zhuang, and V. Bennett. 2019.
884 βII-spectrin promotes mouse brain connectivity through stabilizing axonal plasma
885 membranes and enabling axonal organelle transport.
886 doi:10.1073/pnas.1820649116.

887 Mutalik, S.P., J. Joseph, P.A. Pullarkat, and A. Ghose. 2018. Cytoskeletal
888 Mechanisms of Axonal Contractility. *Biophys. J.* 115:713–724.
889 doi:10.1016/j.bpj.2018.07.007.

890 Nishimura, Y., S. Shi, F. Zhang, R. Liu, Y. Takagi, A.D. Bershadsky, V. Viasnoff,
891 and J.R. Sellers. 2021. The formin inhibitor SMIFH2 inhibits members of the myosin
892 superfamily. *J. Cell Sci.* 134:jcs253708. doi:10.1242/jcs.253708.

893 Qu, Y., I. Hahn, S.E.D. Webb, S.P. Pearce, and A. Prokop. 2017. Periodic actin
894 structures in neuronal axons are required to maintain microtubules. *Mol. Biol. Cell*.
895 28:296–308. doi:10.1091/mbc.e16-10-0727.

896 Ran, F.A., P.D. Hsu, J. Wright, V. Agarwala, D.A. Scott, and F. Zhang. 2013.
897 Genome engineering using the CRISPR-Cas9 system. *Nat. Protoc.* 8:2281–2308.
898 doi:10.1038/nprot.2013.143.

899 Smith, A.S., R.B. Nowak, S. Zhou, M. Giannetto, D.S. Gokhin, J. Papoin, I.C.
900 Ghiran, L. Blanc, J. Wan, and V.M. Fowler. 2018. Myosin IIA interacts with the
901 spectrin-actin membrane skeleton to control red blood cell membrane curvature
902 and deformability. *Proc. Natl. Acad. Sci.* 115:E4377–E4385.
903 doi:10.1073/pnas.1718285115.

904 Unsain, N., M.D. Bordenave, G.F. Martinez, S. Jalil, C. von Bilderling, F.M.
905 Barabas, L.A. Masullo, A.D. Johnstone, P.A. Barker, M. Bisbal, F.D. Stefani, and
906 A.O. Cáceres. 2018. Remodeling of the Actin/Spectrin Membrane-associated
907 Periodic Skeleton, Growth Cone Collapse and F-Actin Decrease during Axonal
908 Degeneration. *Sci. Rep.* 8:3007. doi:10.1038/s41598-018-21232-0.

Vassilopoulos, S., S. Gibaud, A. Jimenez, G. Caillol, and C. Leterrier. 2019. Ultrastructure of the axonal periodic scaffold reveals a braid-like organization of actin rings. *Nat. Commun.* 10:5803. doi:10.1038/s41467-019-13835-6.

Verma, S., N. Kumar, and V. Verma. 2016. Role of paclitaxel on critical nucleation concentration of tubulin and its effects thereof. *Biochem. Biophys. Res. Commun.* 478:1350–1354. doi:10.1016/j.bbrc.2016.08.127.

Wang, G., D.J. Simon, Z. Wu, D.M. Belsky, E. Heller, M.K. O'Rourke, N.T. Hertz, H. Molina, G. Zhong, M. Tessier-Lavigne, and X. Zhuang. 2019. Structural plasticity of actin-spectrin membrane skeleton and functional role of actin and spectrin in axon degeneration. *eLife*. 8:e38730. doi:10.7554/eLife.38730.

Wang, T., W. Li, S. Martin, A. Papadopulos, M. Joensuu, C. Liu, A. Jiang, G. Shamsollahi, R. Amor, V. Lanoue, P. Padmanabhan, and F.A. Meunier. 2020. Radial contractility of actomyosin rings facilitates axonal trafficking and structural stability. *J. Cell Biol.* 219:e201902001. doi:10.1083/jcb.201902001.

Wernert, F., S.B. Moparthi, F. Pelletier, J. Lainé, E. Simons, G. Moulay, F. Rueda, N. Jullien, S. Benkhelifa-Ziyyat, M.-J. Papandréou, C. Leterrier, and S. Vassilopoulos. 2024. The actin-spectrin submembrane scaffold restricts endocytosis along proximal axons. *Science*. 385:eado2032. doi:10.1126/science.ado2032.

Witte, H., D. Neukirchen, and F. Bradke. 2008. Microtubule stabilization specifies initial neuronal polarization. *J. Cell Biol.* 180:619–632. doi:10.1083/jcb.200707042.

Xu, K., G. Zhong, and X. Zhuang. 2013. Actin, Spectrin, and Associated Proteins Form a Periodic Cytoskeletal Structure in Axons. *Science*. 339:452–456. doi:10.1126/science.1232251.

Zhong, G., J. He, R. Zhou, D. Lorenzo, H.P. Babcock, V. Bennett, and X. Zhuang. 2014. Developmental mechanism of the periodic membrane skeleton in axons. *eLife*. 3:e04581. doi:10.7554/eLife.04581.

Zhou, R., B. Han, R. Nowak, Y. Lu, E. Heller, C. Xia, A.H. Chishti, V.M. Fowler, and X. Zhuang. 2022. Proteomic and functional analyses of the periodic membrane skeleton in neurons. *Nat. Commun.* 13:3196. doi:10.1038/s41467-022-30720-x.

Zhou, R., B. Han, C. Xia, and X. Zhuang. 2019. Membrane-associated periodic skeleton is a signaling platform for RTK transactivation in neurons. *Science*. 365:929–934. doi:10.1126/science.aaw5937.

AUTHOR CONTRIBUTIONS

Conceptualisation: S.B. and A.G.; Investigation and formal analysis (all experiments other than laser ablation experiments): S.B.; Investigation and formal analysis (laser ablation experiments): S.B. and A.M.; Methodology and resources: S.B., A.M., P.P. and A.G.; Writing – original draft: S.B. and A.G.; Writing – review and editing: S.B., A.M., P.P. and A.G.; Funding Acquisition: A.G., P.P.

All authors gave final approval for publication and agreed to be held accountable for the work performed therein.

FUNDING

This work was supported by grant no.: IA/TSG/20/1/600137 from DBT-Wellcome Trust India Alliance, grant no.: DST/INT/Portugal/P-04/2021(G) from the Dept. of Science & Technology, Govt. on India and intramural funds from IISER Pune.

ACKNOWLEDGEMENTS

The IISER Pune Microscopy Facility is acknowledged for access to imaging systems and software. We thank Dr. Sayantan Majumdar, RRI Bengaluru, for providing the high-speed camera used in the laser ablation experiments.